TITLE:

DIFFERENTIAL EFFECTS OF REACTIVE OXYGEN SPECIES ON AUTOPHAGY IN ARABIDOPSIS

RUNNING TITLE:

Redox regulation of autophagy

AUTHORS:

Alejandro Enet [1†], Germán Robert [1,2,3 † *], Laura Saavedra [1], Ramiro Lascano [1,2 *]

† Both authors contributed equally

*** Corresponding authors:**

robert.german@inta.gob.ar; ramiro.lascano@unc.edu.ar

AFFILIATIONS

[1] Plant Stress Biology Group, Unidad de Doble Dependencia INTA-CONICET (UDEA), Av. 11 de Septiembre, Córdoba 4755-X5020ICA, Argentina.

[2] Cátedra de Fisiología Vegetal, Facultad de Ciencias Exactas Físicas y Naturales, Universidad Nacional de Córdoba, Av. Velez Sarsfield 299, Córdoba, Argentina;

[3] Instituto Nacional de Tecnología Agropecuaria (INTA), Instituto de Fisiología y Recursos Genéticos Vegetales (IFRGV), Av. 11 de Septiembre, Córdoba 4755-X5020ICA, Argentina.

Alejandro Enet: ale.403@hotmail.com
Germán Robert: robert.german@inta.gob.ar
Laura Saavedra: saavedra.laura@inta.gob.ar
Ramiro Lascano: ramiro.lascano@unc.edu.ar

KEYWORDS

Autophagy, stress, reactive oxygen species, singlet oxygen, superoxide radical, hydrogen peroxide, redox state, Arabidopsis thaliana.

Word count: 4293

Number of figures: 5

Supplementary figures: 7

Date of submission: August 11, 2023

HIGHLIGHT

This research show that the differential effects of ROS on autophagic flux correlates with their effects on cytoplasmic redox state.

ABSTRACT

Autophagy plays a key role in the responses to different stress condition in plants, providing both pro-life and pro-death functions. Reactive oxygen species (ROS), are common modulators of stress responses, having both toxic and signaling functions. In this context, the relationship between ROS and autophagy regulation remains unclear, and in some aspect contradictory. In this study, we employed pharmacological and genetic approaches to investigate the effects of radical superoxide (O_2^-), hydrogen peroxide (H_2O_2) and singlet oxygen ($^1O_2$) on the cytoplastic redox state and autophagic flux in Arabidopsis thaliana. Ours results demonstrated that oxidative treatments with H2O2 and MV, which drastically increased the oxidized state of the cytoplasm, reduced the autophagic flux. Conversely, singlet oxygen, which did not have significant effects on the cytoplasmic redox state, increased the autophagic flux. Additionally, our findings indicated that after H2O2 and high light treatments and during the recovery period, the cytoplasm returned to its reduced state, while autophagy was markedly induced. In summary, our study unveils the differential effects of ROS on the autophagic flux, establishing a correlation with the redox state of the cytoplasm. Moreover, it emphasizes the dynamic nature of autophagy in response to oxidative stress and the subsequent recovery period.

KEYWORDS

Autophagy, stress, reactive oxygen species, singlet oxygen, superoxide radical, hydrogen peroxide, redox state, Arabidopsis thaliana.

ABBREVIATIONS

ATG: autophagy genes
Conc A: Concanamicina A
GFP: green fluorescent protein
GSH: reduced glutathione
GSSG: oxidized glutathione
MV: methyl viologen
roGFP: redox-sensitive green fluorescent proteins
ROS: reactive oxygen species

INTRODUCTION

Plants as sessile organisms are constantly exposed to different biotic and abiotic stress conditions, so they have evolved integrated defense and acclimation mechanisms to cope with adverse conditions. A common effect induced in plants by different stress conditions is the increase in the generation of reactive oxygen species (ROS), such as superoxide (O_2^-), hydrogen peroxide (H_2O_2), singlet oxygen ($^1O_2$), and the hydroxyl radical (-OH), at different subcellular compartments, such as chloroplasts, mitochondria, peroxisomes, cytosol and the apoplast (Apel and Hirt, 2004). ROS are potent oxidants, that depending on their intensity, duration, and location site of production within the cell can modify different biomolecules, affecting the redox state in different subcellular compartments, provoking oxidative stress, inducing senescence symptoms and cell death (Apel and Hirt, 2004; Trippi *et al.*, 2009; Muñoz *et al.*, 2012; Robert *et al.*, 2018). Furthermore, due to their high reactivity and toxicity, the maintenance of tightly regulated ROS levels becomes crucial for plant acclimation, adaptation, and survival, facilitated by the activity of a sophisticated plant antioxidative system. In this way, controlling the different types of ROS produced, their intensity, duration, and site of production has different implications in modulating growth, development, and stress responses (Melchiorre *et al.*, 2009; Miller *et al.*, 2009; Robert *et al.*, 2009). Consequently, ROS are recognized as critical signaling molecules, and the cellular redox state is considered an intensive property of the living system that integrates information from metabolic and environmental cues controlling plant growth and acclimation responses, as well as cell suicide events (Breusegem et al., 2001; Vranova et al., 2002; Breusegem & Dat, 2006; Miller et al., 2008; Baxter *et al.*, 2014; Choudhury *et al.*, 2017; Fichman and Mittler, 2020).

In plants, chloroplast, mitochondria and peroxisome, which are redox active organelles where carbon and energetic metabolisms take place, are major sources of ROS production (Apel and Hirt, 2004). In chloroplasts, the photosynthetic process involves physical, biophysical, and biochemical redox reactions with different reaction rates. In consequence, oxygen became a potent univalent electron or energy acceptor from highly activated intermediates under conditions of excess excitation energy (EEE) (Karpinski *et al.*, 1999). ROS produced in the chloroplasts are particularly important in the retrograde signaling of EEE conditions, affecting nuclear gene expression, acclimation responses as well as programmed cell death (Karpinski *et al.*, 1999; Breusegem *et al.*, 2001; Breusegem and Dat, 2006; Bechtold *et al.*, 2008; Fichman and Mittler, 2020).

Likewise, several stress conditions in plants have been also shown to be capable of triggering or increasing autophagy (Signorelli *et al.*, 2019; Wang *et al.*, 2021). Autophagy is an ancient and conserved process in eukaryotes by which different cellular components are delivered to vacuole/lysosome to be degraded, and is essential for plant energetic metabolisms, growth, development and response to different stress conditions (Su *et al.*, 2020; Wang *et al.*, 2021). Different types of autophagy have been identified in plants (Yoshimoto, 2012). Macroautophagy (hereafter termed autophagy) is the type of autophagy most thoroughly studied in all organisms. The autophagic process is initiated, and mainly modulated in the cytosol, by the formation of a double membrane cup, the phagophore, that expands to engulf macromolecules and cellular components to finally form a double-membrane vesicle called autophagosomes. The autophagosomes are then transported and fused with the vacuole, facilitating the delivery of their cargo for subsequent degradation (Yoshimoto, 2012; Yoshimoto and Ohsumi, 2018). The several steps of the autophagic process are coordinated by ATG

(AuTophaGy) proteins as well as by some components of the endosome pathway, as recently reported (Zhuang *et al.*, 2015; Yoshimoto and Ohsumi, 2018; Robert *et al.*, 2021). While early evidence pointed to a strong transcriptionally regulation of autophagy in response to nutritional starvation conditions and foliar senescence (Yoshimoto *et al.*, 2004; Breeze *et al.*, 2011), recent studies have shed light on the widespread modulation of autophagy initiation and progression by post-translational modifications of core autophagy proteins. These modifications primarily occur at the cytoplasmic level in response to environmental cues (Feng *et al.*, 2015; Yang *et al.*, 2019; Qi *et al.*, 2021).

It has been suggested a positive correlation between ROS generation and the autophagic process, where ROS can serve as both sources of damage and signals (Xiong *et al.*, 2007*a*,*b*; Signorelli *et al.*, 2019). Autophagy promotes the degradation of ROS-overproducing damaged organelles including chloroplasts, mitochondria, and peroxisomes, thus fulfilling antioxidant roles (Xiong *et al.*, 2007*b*; Shibata *et al.*, 2013; Nakamura *et al.*, 2018; Oikawa *et al.*, 2022). Supporting this notion, observations in different autophagy-mutant plants demonstrate the accumulation of oxidized and ubiquitinated proteins (Xiong *et al.*, 2007*a*; Munch *et al.*, 2014), high levels of H_2O_2 (Yoshimoto *et al.*, 2009), increased amounts of total glutathione (Masclaux-Daubresse *et al.*, 2014), accelerated senescence (Doelling *et al.*, 2002; Hanaoka *et al.*, 2002; Yoshimoto *et al.*, 2004), and hypersensitivity to different stress conditions including oxidative stresses (Xiong *et al.*, 2007*b*; Liu *et al.*, 2009; Zhou *et al.*, 2013), indicating a significant redox imbalance. On the other hand, oxidative treatments with H_2O_2 and methyl viologen (MV) have been shown to induce autophagy (Xiong *et al.*, 2007*b*; Pérez-Pérez *et al.*, 2012*b*). Likewise, autophagosome formation triggered by nutritional starvation and saline stress in Arabidopsis roots depends on the NADPH-oxidase complex, a major source of ROS in the apoplast, which is essential for local and systemic redox signal transduction (Liu *et al.*, 2009). However, the induction of autophagy under osmotic stress was shown to be NADPH oxidase-independent, suggesting that different signaling pathways regulate autophagy induction, and in certain scenarios are dependent on ROS signaling (Liu *et al.*, 2009). More recently, it has been hypothesized that H_2O_2 accumulation and membrane damage may mediate chlorophagy induced by UV and high light treatments in Arabidopsis leaves (Izumi *et al.*, 2017; Woodson, 2019). Consequently, it is plausible that autophagy induction occurs as a response to the accumulation of cellular components that have been damaged. Notably, recent studies conducted in yeast, animals and Chlamydomonas have revealed that certain proteins involved in the autophagic process could be inhibited by ROS in *in vitro* experiments or artificial oxidative stress *in vivo*, indicating that ROS may inhibit the function of some autophagy-related proteins (Pérez-Pérez *et al.*, 2014, 2016; Frudd *et al.*, 2018). These findings raise apparently opposite evidence regarding the redox regulation of autophagy. Hence, the picture about the relationship among different ROS, subcellular redox changes, and autophagy regulation in plants is still unclear. Under this scenario, our study aimed to address the effects of different ROS on autophagy in plants.

Herein, we provide evidence that oxidative treatments with H_2O_2 and MV, which drastically increased the oxidized state of the cytoplasm, led to a reduction in the autophagic flux in Arabidopsis seedlings. Likewise, after the oxidative treatments and during the subsequent recovery period, the cytoplasm returned to its reduced state while autophagy was markedly induced. On the other hand, pharmacological and genetic approaches that enhance the generation of $^1O_2$ resulted in an increased autophagic flux in Arabidopsis seedlings, but no significant effects were observed on the cytoplasmic redox state. In summary, our findings unveil the distinct effects of ROS on the autophagic flux, highlighting a strong correlation between the oxidized state of the cytoplasm and the inhibition of autophagy.

MATERIALS AND METODS

Plant materials and growth conditions.

Arabidopsis thaliana ecotype Columbia (Col-0) was used in this study. 35S:GFP-ATG8a transgenic seeds (CS39996) (Thompson et al., 2005) were obtained from the Arabidopsis Biological Resource Center. The cytosol-targeted fluorescent redox sensors GFP2-Orp1 or GRX-roGFP2 were provided by Dr. Markus Schwarzländer. Fluorescent (*flu*) and ferrochelatase 2 (*fc2*) mutants were provided by Dr. Jesse Woodson. We introgressed the GFP-ATG8a, GFP2-Orp1 and GRX-roGFP2 transgenes into the *flu* and *fc2* mutant lines by genetic crosses. Homozygous offspring were then selected from the F3 backcross generations.

Seeds were surface-sterilized and sown on culture plates containing nutrient-rich Murashige and Skoog (MS) solid medium lacking sucrose and containing 1 % agar. After sowing, plates were kept in darkness at 4°C for 2 to 3 days, and then transferred to a growth chamber under a 16 h light/8 h dark photoperiod. Photosynthetic photon flux density was 110 µmol m^{-2} sec^{-1}. Average temperature was 22°C. Plants were grown for 7 days under these conditions and then passed to MS liquid medium to carry out the different treatments. For salt and osmotic stresses, NaCl (50 mM) and mannitol (100 mM) were used, respectively. Oxidative treatments were performed by the supplementation of the MS liquid medium with 1 µM methyl viologen (MV), 10 mM H_2O_2, 20 µM 3-(3,4-dichlorophenyl)-1,1-dimethylurea (DCMU), 20 µM methylene blue (MB). To scavenge superoxide and peroxide, 10 mM tiron and 10 mM benzoic acid (BA) were co-administrated, respectively. 10 mM dithiothreitol (DTT) was used as a reducing agent for protein disulfide bonds.

Confocal fluorescence microscopy and image analysis.

Confocal microscopy was performed on an Inverted microscope Nikon Eclipse CZ1. 35S:GFP-ATG8a expressing plants were observed with a 488-nm argon laser (BP 495–530 nm). To analyze autophagic bodies accumulation, 1 µM Concanamycin A was added to the different treatments. The number of autophagic bodies in epidermal cells was quantified after 16 h of treatments using ImageJ by counting their numbers in the central vacuole of multiple cells in sections of 2500 $µm^2$. Cytosol-targeted fluorescent redox sensors GFP2-Orp1 or GRX-roGFP2 were excited at 488 nm and 405 nm and fluorescent emissions were collected at 505-535 nm. Subsequently, a single ratiometric image was generated using the ImageJ software, where the value of each pixel is the product of the ratio between the intensity at 405 nm with respect to that obtained at 488 nm. For pseudocolor display, the ratio was coded on a spectral color scale ranging from blue (fully reduced) to red (fully oxidized).

Immunoblot analyses.

Seven-day old 35S:GFP-ATG8a transgenic plants were transferred to MS liquid medium to carry out the different treatments for 6 h. Then, total proteins were extracted. The extracts were centrifuged at 10 000 g for 10 min, and equal amounts of proteins from the supernatants were subjected to SDS-PAGE and immunoblotted with anti-GFP antibodies (Roche).

Physiological parameters.

Seven-day old Arabidopsis seedlings were exposed to the different treatments for 8 h and then the production of H_2O_2 and O_2^-, quantum efficiency of PSII photochemistry (ΦPSII), as well as the content of chlorophyll, soluble sugars and malondialdehyde (MDA) were analyzed. To assess H_2O_2 and O_2^- accumulation, leaves were stained with DAB and NBT, respectively. The staining was quantified by measuring the intensity per area using ImageJ. Quantum efficiency of PSII photochemistry (ΦPSII) was measured from the upper surface using a pulse amplitude modulated fluorometer (FMS2, Hansatech Instruments, Pentney King's Lynn, UK). Measurements were performed 6 h after the growth chamber lights were turned on. For chlorophyll, soluble sugars, and MDA analysis an alcoholic extract (1:2 w/v) was obtained from the samples. After centrifugation for 15 minutes at 12,000 *g*, the supernatant was diluted in ethanol, and the absorbance was measured at 654 nm using a spectrophotometer. Total chlorophylls were calculated following the method reported by (Wintermans M. and De Mots A., 1965). For soluble sugars determination, an aliquot of the sample was dried, and resuspended in a same volume of water. Then, the concentration of sugars was measured with anthrone (Fales, 1951) evaluating the absorbance at 620 nm using a glucose standard curve. For MDA determination, a volume of the supernatant was mixed with a same volume of a mixture of 0,5 % TBA and 20 % TCA, and incubated 20 minutes at 90 °C. The mixture was centrifuged at 12,000 *g* for 5 minutes, and the absorbance was measured at 532 and 600 nm (Heath and Packer, 1968).

RNA extraction and RT-qPCR

Samples were homogenized in a cold mortar with TRIzol Reagent, mixed for 1 min and incubated at room temperature for 5 min. Then, 0.2 ml chloroform per ml of TRIzol Reagent was added and incubated at room temperature for 3 min. After incubation, the samples were centrifuged at 12 000 *g* at 4 °C for 15 min and the aqueous phases were transferred to clean tubes. RNA was precipitated by adding 1 vol of isopropanol, incubated at room temperature for 10 min and centrifuged at 12 000 *g* at 4 °C for 15 min. The precipitate was washed with 70 % ethanol and the samples were centrifuged again at 12 000 *g* at 4 °C for 15 min. The precipitates were dried and resuspended in diethyl pyrocarbonate-treated water and its concentration was quantified using a NanoDrop 3300 spectrometer (Thermo Scientific). Purified RNA was treated with DNase I (Invitrogen) to remove genomic DNA, according to the manufacturer's instructions. DNA-free RNA (1 to 2.5 µg) was used with oligo(dT) for first strand cDNA synthesis using the Moloney murine leukemia virus reverse transcriptase (M-MLV RT, Promega) according to the manufacturer's instructions. For each primer pair, the presence of a unique product of the expected size was checked on ethidium bromide-stained agarose gels after PCR reactions. Absence of contaminant genomic DNA was confirmed in reactions with DNase-treated RNA as template. The qPCR reaction was performed using iQ Universal SYBR Green Supermix (Bio-Rad). Amplification of actin with the forward primer 5'-TTCAGATGCCCAGAAGTCTTG-3' and the reverse primer 5-GCGATACCTGAGAACATAGTGG-3 was used to normalize the amount of template cDNA. The specific primers pair employed for the detection of *Atg6* was forward primer 5'-AAAACTGGGAGAGCGATGAG-3' and reverse primer 5'-GATAGATGAGCCCTGCGTAG-3', for *Atg4a* was 5'-CCTTTGGAATCACTCGACCCATCT-3' and 5'-ATCCGCAAACCCGTAGTTGCTT-3', for *Atg7* was 5'-GCGGCTTTAGGTTTTGACAG-3' and 5'-GTTGGTCTAGAGTTCGATCAGTC -3', and for *Atg5* was 5'-TCCTGTTCGGTTGTATGTTCG-3' and 5'-CGCTCTGTCTCCCATAAACTC-3'. qPCR was performed in thermocycler iQ5 (Bio-Rad) at 59 °C with iQ SYBR Green Supermix (Bio-Rad), according to the manufacturer's instruction. Relative transcript abundance was calculated (Livak and Schmittgen, 2001).

Microarray analysis.

Publicly available microarray data were utilized to compare the expression of *Atg* genes under various conditions, including nitrogen deficiency (Rubin *et al.*, 2009), treatment with 10 mM H_2O_2 for 24 h (Willems *et al.*, 2016), treatment with 10 µM MV for 2 h (Scarpeci *et al.*, 2008), and the examination of *flu* mutant plants subjected to an 8-hour cycle of darkness followed by 2 h of light (Op Den Camp *et al.*, 2003). Expression values were normalized to the corresponding control conditions employed in each study and were expressed as $\log_2$ values.

Statistical analyses.

Data were analysed by analysis of variance (ANOVA) followed by the Di Rienzo–Guzman–Casanoves (DGC) test model, a cluster-based method for identifying groups of non-homogeneous means, using InfoStat software (Di Rienzo *et al.*, 2002).

RESULTS

Methyl viologen and H_2O_2 oxidized the cytoplasmic redox state and inhibited autophagy in Arabidopsis.

To gain insights into the interplay between ROS and autophagy, *Arabidopsis thaliana* seedlings were subjected to well-established autophagy-inducing conditions, namely nutritional starvation and different abiotic stress treatments (Wang *et al.*, 2021), and both autophagy and the cytoplasmic redox state were analyzed (Fig. 1). To monitor autophagy, 35S:GFP-ATG8a (GFP-ATG8) transgenic plants were grown 7 days in MS solid medium, and then transferred to the different treatments in MS liquid medium supplemented with 1 µM Concanamycin A (Conc A) for a 16 hour-period. Conc A is a V-ATPase inhibitor widely used to prevent vacuole acidification, thereby effectively inhibiting the lytic activity of vacuoles, thus allowing the detection of autophagic bodies accumulation into the vacuoles through confocal microscopy (Fig. 1A and B). Analysis of autophagic flux using Conc A better defines autophagic activity since the increase of autophagosome number in the cytoplasm does not necessarily corresponds to an enhanced autophagic activity (Robert *et al.*, 2021). When subjected to carbon and nitrogen starvation treatments, epidermal cells showed a high accumulation of autophagic bodies in the vacuole compared to control conditions, indicating an activated autophagic flux (Fig. 1A and B). Similarly, saline and osmotic stress treatments resulted in comparable outcomes, with a significant increase in autophagic bodies accumulating within the vacuoles (Fig. 1A and B). Besides, to evaluate the cytoplasmic redox state *in vivo*, 7 days old transgenic plants expressing the cytosol-targeted fluorescent redox sensors GFP2-Orp1 or GRX-roGFP2 were subjected to the different treatments (Fig. 1). These transgenic plants express redox-sensitive green fluorescent proteins (roGFPs) genetically fused to different redox-active proteins sensing H_2O_2 production and GSH:GSSG, respectively (Aller *et al.*, 2013; Nietzel *et al.*, 2019). The relative intensity of the two fluorescence excitation maxima depends on the redox state of the modified GFP, enabling ratiometric measurements, independent of the probe concentration (Schwarzländer *et al.*, 2016). Notably, in epidermal cells of seedlings expressing either GFP2-Orp1 or GRX-roGFP2, no changes in the cytoplasmic redox state were detected after 16 h of nutritional starvation, saline or osmotic stress treatments compared to control conditions (Fig. 1A and C).

To further investigate the interplay between ROS and autophagy, oxidative stress treatments using methyl viologen (MV) and H_2O_2 were conducted. MV is an herbicide that generates O_2^- and H_2O_2 in the presence of light inside chloroplasts (Lascano *et al.*, 2012). Previously, we evaluated different concentrations of MV and H_2O_2 (Fig. S1 and Fig. S2, respectively). For the subsequent experiments, we used 1 µM MV since it was the lowest concentration that showed effects on the cytoplasmic redox state (Fig. S1). Although oxidative treatments have been reported as autophagy-inducing conditions in Arabidopsis and Chlamydomonas (Xiong *et al.*, 2007*b*; Pérez-Pérez *et al.*, 2012*b*), no significant differences were observed in the accumulation of autophagic bodies in the epidermal cells of seedlings treated with MV or H_2O_2 compared to the control condition (Fig. 1A and B). Interestingly, contrary to the observations under nutritional starvation, saline or osmotic stresses, these oxidative treatments were able to significantly oxidize both biosensors indicating an increase in H_2O_2 levels and GSSG:GSH ratio in the cytoplasm (Fig. 1A and C).

To further characterize the effects of oxidative stress on autophagy, treatments with MV and H_2O_2 were performed on 35S:GFP-ATG8a plants under autophagic inducing conditions, specifically nitrogen and carbon starvation (Fig. 2). Interestingly, treatments with MV and H_2O_2 reduced the accumulation of autophagic bodies after 16 h of starvation conditions (Fig. 2A and B). Furthermore, the inhibitory effects of the oxidative treatments on the autophagic flux were also confirmed by analyzing the degradation of the GFP-ATG8a fusion protein by western blot (Fig. 2D). The evaluation of autophagic flux through the analysis of the degradation of the GFP-ATG8 fusion protein by immunoblotting allowed us to examine the effects of oxidative stress on autophagy in shorter time periods (6 h, Fig. 2D). Next, to scavenge superoxide and peroxide, tiron and benzoic acid were co-administered with the MV treatment. The oxidative effects of MV on the autophagic flux (Fig. 2A, B and D) and the cytoplasmic redox state (Fig. 2B and C) were blocked in the presence of ROS scavengers. Similarly, photooxidative treatments showed an inhibitory effect on the autophagy flux, which was reversed in the presence of the superoxide radical scavenger, tiron (Fig. 2D). Moreover, both tiron and benzoic acid reduced the accumulation of H_2O_2 and O_2^- generated under oxidative stress, as indicated by DAB and NBT staining, respectively (Fig. 2E), as well as prevented photosynthetic damage caused by MV treatments, as measured by the quantum efficiency of photosystem II (ΦPSII) (Fig. 2F). Besides, the scavenging of O_2^- by the administration of tiron also prevented the decrease in soluble sugar levels that was observed in the MV treatments (Fig. 2G). Furthermore, the inhibitory effects of MV on autophagic flux and the oxidation of the GSH:GSSG sensor probe (GRX-roGFP2) were reversed when 10 mM dithiothreitol (DTT), a reducing agent for protein disulfide bonds, was added (Fig. S3). Nevertheless, DTT treatments exhibited slight effects on H_2O_2 production compared to tiron treatments (Fig. S3). These results emphasize that the effects of MV in plants are associated to its ability to promote the generation of ROS, contributing to a more oxidized cellular redox state and oxidative damage (Lascano *et al.*, 2012). It is noteworthy that the effect of tiron, benzoic acid, and DTT in restoring the autophagic flux in MV-treated plants suggested that H_2O_2 may inhibit autophagy, potentially by oxidizing disulfide bonds in key ATG proteins (Fig. S4 and S5) as demonstrated in recent studies in yeast, Chlamydomonas and animals (Pérez-Pérez *et al.*, 2014, 2016; Frudd *et al.*, 2018; Zheng *et al.*, 2020). In this regard, the inhibitory effect of H_2O_2 on autophagy was also observed in plants subjected to carbon or nitrogen starvation (Fig. 2A, B and D; Fig. S2).

Autophagy is induced in the recovery phase after oxidative stress in Arabidopsis.

Previous reports indicated that autophagy is involved in degrading oxidized proteins and organelles in response to oxidative stress (Xiong *et al.*, 2007*b*; Shibata *et al.*, 2013; Izumi *et al.*, 2017; Oikawa *et al.*, 2022). However, our experimental results demonstrate that oxidative stress treatments inhibit autophagy, as illustrated in Figure 2. Considering these findings, we aimed to investigate the autophagic activity following oxidative stress treatments by evaluating the autophagic flux in Arabidopsis plants during the recovery phase. With this purpose, 7-day-old

Arabidopsis seedlings were subjected to a brief exposure of 10 mM H_2O_2 or high light intensity (≈1000 µmoles m^{-2} s^{-1}) for 4 hours, followed by transfer to H_2O_2-free MS liquid medium for a 20-hour recovery period. Additionally, a set of plants were incubated in 10 mM H_2O_2 or to control conditions (H_2O_2-free MS liquid medium) for 24 h. This experimental design aimed to elucidate the dynamic changes in autophagy following oxidative stress and determine whether autophagic activity is modulated during the recovery phase. The results showed that autophagic flux was inhibited in plants incubated 24 h with H_2O_2 compared to control conditions (Fig. 3A, B and D). However, autophagic flux was not only recovered but also induced during the recovery period after the stress treatments surpassing the levels observed in plants subjected to control conditions (Fig. 3A, B and D). Likewise, after the 20-hour recovery period, the redox biosensors returned to their reduced state, indicating both a successful cytoplasmic redox recovery, and a clear correlation between reduced cytoplasmic redox state and autophagic flux (Fig. 3A and C).

Singlet oxygen induced autophagic flux but did not affect the cytoplasmic redox state.

Singlet oxygen ($^1O_2$) is mainly produced in the chloroplast, and its targets are predominantly confined inside this organelle due to the specific physicochemical characteristic of this ROS (Dmitrieva *et al.*, 2020). To investigate the effects of $^1O_2$ on the autophagic activity, GFP-ATG8a seedlings were incubated with 3-(3,4-dichlorophenyl)-1,1-dimethylurea (DCMU) (Fig. 4), an herbicide that blocks plastoquinone reduction promoting $^1O_2$ generation at the PSII (Flors *et al.*, 2006), and the accumulation of autophagic bodies and cytoplasmic redox state were analyzed after 16 h (Fig. 4A-C). Additionally, treatments with methylene blue (MB), a type-II photosensitizer able to generate $^1O_2$ in leaves under visible light, with minor effects on photosynthesis (Fig. 4E), were also performed. Treatments with these chemicals increased the accumulation of autophagic bodies but did not show statistically significant effects on the redox state of the cytoplasm in Arabidopsis cells compared to control treatment (Fig. 4A and C) (Fig. 4A and B). The autophagic flux-inducing effect of DCMU and MB was also evidenced after 6 hours of treatments through the analysis of GFP-ATG8 degradation by immunoblotting (Fig. 4D).

To further investigate the effects of $^1O_2$ on the autophagic process and the cytoplasmic redox state, autophagy reporter- and redox sensor-transgenic plants were crossed with widely used endogenously chloroplast $^1O_2$-hyperproducing *Arabidopsis* mutant plants: fluorescent (*flu*) and two different lines of ferrochelatase 2 (*fc2*), *fc2.1* which presents reduced expression levels of *Fc2*, and the null mutant *fc2.2*. These mutant plants accumulate different photosensitizing intermediates of chlorophyll biosynthesis in the dark, which, upon light exposure lead to an exacerbated production of $^1O_2$ (Flors *et al.*, 2006). The *flu* mutant plants accumulate protochlorophyllide (Meskauskiene *et al.*, 2001), while mutations in plastid ferrochelatase 2 lead to the accumulation of protoporphyrin IX (Scharfenberg *et al.*, 2015). Initially, wild type, *flu* and *fc2* mutant plants were grown 7 days under continuous light conditions (control conditions), and several growth and physiological parameters were evaluated (Fig. S6). Interestingly, the *fc2* mutants showed arrested root growth, reduced chlorophyll levels, increased levels of MDA and reduced levels of soluble sugars compared to wild type, while no significant differences were observed between wild type and *flu* mutant (Fig. S6). Likewise, the cytoplasmic redox state in *fc2* plants was significantly more oxidized than that in the wild type and *flu* backgrounds (Fig. S6, Fig. 5). Furthermore, and consistent with a previous study (Lemke *et al.*, 2021), the autophagic flux was induced in *fc2* mutants plants compared to wild type and *flu* mutant under continuous light conditions (Fig. S6). Hence, considering the altered phenotypes observed in *fc2* mutants even under control conditions, we used the *flu* mutants for subsequent analysis.

flu/GFP-ATG8a plants were grown under continuous light conditions for 7 days, transferred to darkness for 8 h, and then re-exposed to light in the presence of Conc A for another 8 h. After the light/dark/light cycling conditions, a significantly increased autophagic flux was observed in *flu*/GFP-ATG8a compared to Col-0/GFP-ATG8 plants. However, no statistically significant differences were observed among these genotypes under continuous light conditions (Fig. 5A, B and D). Besides, the cytoplasmic redox state was monitored under control conditions as well as after a period of darkness by analyzing the fluorescent redox sensor roGFP2-ORP1 expressed in the wild type and *flu* backgrounds. Although a slight tendency towards a more oxidized state was observed in the cytoplasm of *flu* mutant plants once re-exposed to light, the differences were not statistically significant (Fig. 5C). Thus, in contrast to H_2O_2 and MV treatments, $^1O_2$ increased the autophagic flux and did not oxidize the cytoplasmic redox state, indicating differential effects on the autophagic activity depending on the ROS nature and their effects on the cytoplasmic redox state. Moreover, the transcript levels of *Atg4*, *Atg5*, *Atg6* and *Atg7* were analyzed by RTq-PCR in *flu* mutant after 8 h of light re-exposure. However, no statistically significant differences were observed in the expression level of the analyzed genes between wild type and *flu* mutant neither under control conditions nor after cycling conditions (Fig. S7).

DISCUSSION

Plants, as aerobic and sessile organisms, respond to environmental stresses by increasing the production of reactive oxygen species (ROS), which, due to their high reactivity, fulfill dual roles by acting both as agents of damage and as signaling molecules. Consequently, ROS are universally implicated in plant stress symptomatology, and also play a pivotal role in modulating plant growth, development, and cell death (Apel and Hirt, 2004; Trippi *et al.*, 2009). Similarly, a multitude of stress conditions in plants have been demonstrated to initiate or enhance autophagy (Bassham *et al.*, 2006; Liu *et al.*, 2009; Signorelli *et al.*, 2019; Su *et al.*, 2020). Moreover, defects in antioxidant proteins in Arabidopsis and Chlamydomonas contribute to uncontrolled ROS bursts and autophagy induction (Pérez-Pérez *et al.*, 2012*a*; Shibata *et al.*, 2013). While the concurrent induction of ROS production and autophagy activation suggests a positive correlation between these cellular processes, certain molecular mechanisms have been reported in animal cells, yeast, and Chlamydomonas, indicating that ROS could potentially exert a negative influence on autophagy (Pérez-Pérez *et al.*, 2014, 2016; Frudd *et al.*, 2018). However, direct evidence of ROS-mediated inhibition of autophagy remains scarce in plants. One of the fundamental unanswered queries is whether a particular type of ROS functions as the primary messenger, if any, to induce autophagy. Our findings point in that direction, highlighting the differential effects of ROS on autophagy and suggesting that, under specific stress conditions leading to a highly oxidized cytoplasmic state, the autophagic process may be suppressed.

In this study, MV was used to specifically generate O_2^- and H_2O_2 in the chloroplast. Previous studies have reported the formation of autophagosomes in root cells following incubation with MV (Xiong *et al.*, 2007*b*). Nevertheless, our findings differ from these outcomes. It is important to acknowledge that certain variations in experimental and methodological approaches between our research and the prior studies may have a considerable impact on the interpretation of the outcomes. In the earlier studies, MV treatments were administered on solid MS media, subjecting plants to 10 µM MV for a duration of two days, and the observations were made in roots (heterotrophic tissues where MV produces O_2^- in mitochondria). Conversely, in our study, MS liquid media was supplemented with 1 µM MV, and leaves were analyzed (tissues where MV generates O_2^- in chloroplast). Furthermore, a critical distinction lies in the method employed for quantifying autophagosomes. Previous investigations employed monodansylcadaverine (MDC) staining to identify acidic compartments. However, experiments involving autophagy-deficient *atg* mutants, as well as co-localization analysis in GFP-ATG8 plants, indicated that the MDC-stained structures do not clearly manifest as autophagosomes and/or autolysosomes (Merkulova et al., 2014). In contrast, we used GFP-ATG8 plants for autophagy analysis, which is a more reliable and widely accepted method for identifying autophagosomes.

The relationship between autophagy and ROS is intricate, and our findings revealed that different types of ROS, even when generated in the same organelle, can have different effects on the autophagic process. We observed that under conditions of nutritional starvation, which are canonical inducers of autophagy, oxidative treatments had an inhibitory effect on the autophagic flux. This implies that the comparatively limited autophagosome biogenesis rate under optimal growth conditions could potentially account for the absence of observable inhibitory effects of ROS on autophagy in prior *in vivo* plant studies. Opposite to the inhibitory effects of H_2O_2 on the autophagic flux, the specific generation of $^1O_2$ in the *flu* mutant plants, as well as treatments with DCMU and MB, increased the autophagic activity. These findings are consistent with previous research demonstrating that treatments with norflurazon, an inhibitor of carotenoid biosynthesis, triggers autophagy in *Chlamydomonas reinhardtii* (Pérez-Pérez *et al.*, 2016). Similarly to what is observed in *flu* mutants (Flors *et al.*, 2006), norflurazon treatments lead to perturbations in plastid homeostasis that increase the photosensitizing activity of tetrapyrroles, which can transfer the excitation energy to the oxygen molecule, thereby generating $^1O_2$ (Kim and Apel, 2013). With a shorter half-life and inability to cross membranes, the activity of $^1O_2$ is confined to the thylakoid membrane of chloroplasts (Dmitrieva *et al.*, 2020). These characteristics provide potential explanations for the absence of observable effects on the cytoplasmic redox state in treatments involving DCMU, MB, and *flu* mutant plants. Conversely, treatments with MV and H_2O_2 highly oxidized the cytoplasmic redox state. These results establish a clear correlation between the cytoplasmic redox state of the cytoplasm and autophagic activity.

The observation that the inhibition of autophagic flux and the oxidation of the cytoplasmic redox state in MV treatments can be prevented by ROS scavengers such as tiron or benzoic acid, as well as by treatment with the disulfide bonds reductant DTT, strengthens the notion that H_2O_2 inhibits autophagy, but also suggests that protein oxidation in the cytoplasm may be involved in this response. Notably, it has been proposed that proteins are the primary targets of reactive oxidants and other radicals *in vivo* (Davies, 2005). At the molecular level, the activity of certain ATG proteins has been shown to be regulated by redox changes. For instance, ATG4, a protein involved in the cleavage of ATG8 for its lipidation and de-lipidation, is inhibited by H_2O_2 in yeast and the green alga *Chlamydomonas reinhardtii* (Pérez-Pérez *et al.*, 2014, 2016). Conversely, reducing agents such as DTT can restore the activity of ATG4 (Pérez-Pérez *et al.*, 2014, 2016). Furthermore, it has been reported in animal cells that oxidation of ATG3 and ATG7 leads to the inhibition of autophagy (Frudd *et al.*, 2018). Although the inhibition of autophagy due to oxidations in ATG3 and ATG7 has not been tested in plants, the conservation of amino acid sequence between the isoforms from yeast, human cells, and Arabidopsis (Fig. S4 and S5) suggest that this type of regulation could also occur in plants.

The complexity of the relationship between autophagy and ROS becomes even more complex when considering that this catabolic process is involved in the degradation of proteins and oxidized organelles, which are primary sources of ROS production. The increased autophagic flux observed during the recovery period after exposure to oxidative stress, accompanied by the restoration of a reduced redox state in the cytoplasm, indicated that the inhibition of autophagy by ROS is transient. By assessing the autophagic flux, we aimed to gain insights into the role of autophagy in cellular adaptation to oxidative stress and its potential contribution to stress recovery mechanisms. Our results suggest that autophagy induction once the oxidative stress has subsided is associated with the intracellular clearance of cytoplasmic components damaged by oxidative stress, as indicated by the experiments with the antioxidants tiron and benzoic acid, which controlled ROS production and prevented cell injury. These observations highlight the dynamic nature of autophagy in response to oxidative stress and its subsequent recovery, suggesting a complex regulatory mechanism in Arabidopsis.

In summary, our work provides a novel perspective on the relationship between ROS and autophagy. The fact that the generation of O_2^-/H_2O_2 and $^1O_2$ have different effects on autophagy imply that the term “ROS” encompasses molecules with the ability to modulate this process in distinct ways. Further studies are needed to unravel the molecular mechanisms underlying the differential modulation of autophagy by ROS, being ATG4, ATG3 and ATG7 possible targets to be oxidatively regulated.

SUPPLEMENTARY DATA

Supplementary Figure 1: Assessment of different MV concentrations.
Supplementary Figure 2: Assessment of different H_2O_2 concentrations.
Supplementary Figure 3: DTT reversed the effects of MV treatments.
Supplementary Figure 4: Sequence alignment of ATG4 proteases from different organisms.
Supplementary Figure 5: Sequence alignment of ATG3 and ATG7 proteins from different organisms.
Supplementary Figure 6: Characterization of *fc2* and *flu* mutant plants under continuous light conditions.
Supplementary Figure 7: Transcript level of *Atg* genes in Arabidopsis plants subjected to different oxidative treatments.

ACKNOWLEDGEMENTS

We thank Dr Leandro Ortega and Dr. Virginia Lobatto (Unidad de Doble Dependencia INTA-CONICET (UDEA)) for helpful support with the confocal microscopy and for technical support, respectively. We also thank Sistema Nacional de Microscopia of the Ministerio de Ciencia, tecnología e innovación Productiva (MINCyT), Argentina.

AUTHOR CONTRIBUTION:

GR and RL: conceptualization; GR, and AE: investigation; GR, AE, LS and RL: formal analysis; GR, LS, and RL: resources; GR and AE: writing - original draft; GR, AE, LS, and RL: writing - review & editing; GR and AE: visualization; GR and RL: supervision; GR and RL: funding acquisition.

CONFLICT OF INTEREST

No conflict of interest declared.

FUNDING

This work was supported by grants from Agencia Nacional de Promoción Científica y Tecnológica, Argentina: FONCYT-PICT-2019-0533 (RL), FONCyT PICT-2017-2863 (GR), and FONCyT PICT-2020-2482 (LS); Consejo Nacional de Investigaciones Científicas y Técnicas CONICET-PIP2015-PIP2019 (RL), Proyecto INTA 2019-PD-E6-I116-001 (RL and GR), and Proyectos Consolidar, Secretaría de Ciencia y Técnica de la Universidad Nacional de Córdoba (UNC) (RL).

REFERENCES

Aller I, Rouhier N, Meyer AJ. 2013. Development of roGFP2-derived redox probes for measurement of the glutathione redox potential in the cytosol of severely glutathione-deficient rml1 seedlings. Frontiers in Plant Science **4**, 1–12.

Apel K, Hirt H. 2004. Reactive oxygen species: metabolism, oxidative stress, and signal transduction. Annual review of plant biology **55**, 373–99.

Bassham DC, Laporte M, Marty F, Moriyasu Y, Ohsumi Y, Olsen LJ, Yoshimoto K. 2006. Autophagy in Development and Stress Responses of Plants. Autophagy **2**, 2–11.

Baxter A, Mittler R, Suzuki N. 2014. ROS as key players in plant stress signalling. Journal of Experimental Botany **65**, 1229–1240.

Bechtold U, Richard O, Zamboni A, Gapper C, Geisler M, Pogson B, Karpinski S, Mullineaux PM. 2008. Impact of chloroplastic- and extracellular-sourced ROS on high light-responsive gene expression in Arabidopsis. Journal of experimental botany **59**, 121–33.

Breeze E, Harrison E, McHattie S, *et al.* 2011. High-resolution temporal profiling of transcripts during Arabidopsis leaf senescence reveals a distinct chronology of processes and regulation. Plant Cell **23**, 873–894.

Breusegem F Van, Dat JF. 2006. Reactive Oxygen Species in Plant Cell Death. Plant physiology **141**, 384–390.

Breusegem F Van, Vranova E, Dat JF, Inze D. 2001. The role of active oxygen species in plant signal transduction. Plant Science **161**, 405–414.

Choudhury FK, Rivero RM, Blumwald E, Mittler R. 2017. Reactive oxygen species, abiotic stress and stress combination. Plant Journal **90**, 856–867.

Davies MJ. 2005. The oxidative environment and protein damage. Biochimica et Biophysica Acta - Proteins and Proteomics **1703**, 93–109.

Dmitrieva VA, Tyutereva E V., Voitsekhovskaja O V. 2020. Singlet oxygen in plants: Generation, detection, and signaling roles. International Journal of Molecular Sciences **21**.

Doelling JH, Walker JM, Friedman EM, Thompson AR, Vierstra RD. 2002. The APG8/12-activating enzyme APG7 is required for proper nutrient recycling and senescence in Arabidopsis thaliana. Journal of Biological Chemistry **277**, 33105–33114.

Fales FW. 1951. The assimilation and degradation of carbohydrates by yeast cells. The Journal of biological chemistry **193**, 113–124.

Feng Y, Yao Z, Klionsky DJ. 2015. How to control self-digestion: transcriptional, post-transcriptional, and post-translational regulation of autophagy. Trends in cell biology **25**, 354–363.

Fichman Y, Mittler R. 2020. Rapid systemic signaling during abiotic and biotic stresses: is the ROS wave master of all trades? Plant Journal **102**, 887–896.

Flors C, Fryer MJ, Waring J, Reeder B, Bechtold U, Mullineaux PM, Nonell S, Wilson MT, Baker NR. 2006. Imaging the production of singlet oxygen in vivo using a new fluorescent sensor, Singlet Oxygen Sensor Green. Journal of experimental botany **57**, 1725–34.

Frudd K, Burgoyne T, Burgoyne JR. 2018. Oxidation of Atg3 and Atg7 mediates inhibition of autophagy. Nature Communications **9**, 1–15.

Hanaoka H, Noda T, Shirano Y, Kato T, Hayashi H, Shibata D, Tabata S, Ohsumi Y. 2002. Leaf senescence and starvation-induced chlorosis are accelerated by the disruption of an Arabidopsis autophagy gene. Plant Physiol **129**, 1181–1193.

Heath RL, Packer L. 1968. Photoperoxidation in isolated chloroplasts. Archives of Biochemistry and Biophysics **125**, 189–198.

Izumi M, Ishida H, Nakamura S, Hidema J. 2017. Entire Photodamaged Chloroplasts Are Transported to the Central Vacuole by Autophagy. The Plant Cell **29**, 377.

Karpinski S, Reynolds H, Karpinska B, Wingsle G, Creissen G, Mullineaux P. 1999. Systemic signaling and acclimation in response to excess excitation energy in Arabidopsis. Science **284**, 654–7.

Kim C, Apel K. 2013. 1O2-mediated and EXECUTER-dependent retrograde plastid-to-nucleus signaling in norflurazon-treated seedlings of arabidopsis thaliana. Molecular Plant **6**, 1580–1591.

Lascano R, Munoz N, Robert G, Rodriguez M, Melchiorre M, Trippi V, Quero G. 2012. Paraquat: An Oxidative Stress Inducer. Herbicides - Properties, Synthesis and Control of Weeds. London: IntechOpen, 135–148.

Lemke MD, Fisher KE, Kozlowska MA, Tano DW, Woodson JD. 2021. The core autophagy machinery is not required for chloroplast singlet oxygen - mediated cell death in the Arabidopsis thaliana plastid ferrochelatase two mutant. BMC plant biology **21**, 1–20.

Liu Y, Xiong Y, Bassham DC. 2009. Autophagy is required for tolerance of drought and salt stress in plants. Autophagy **5**, 954–63.

Livak KJ, Schmittgen TD. 2001. Analysis of relative gene expression data using real-time quantitative PCR and the 2(-Delta Delta CT) Method. Methods **25**, 402–408.

Masclaux-Daubresse C, Clement G, Anne P, Routaboul J-M, Guiboileau A, Soulay F, Shirasu K, Yoshimoto K. 2014. Stitching together the Multiple Dimensions of Autophagy Using Metabolomics and Transcriptomics Reveals Impacts on Metabolism, Development, and Plant Responses to the Environment in Arabidopsis. The Plant Cell **26**, 1857–1877.

Melchiorre M, Robert G, Trippi V, Racca R, Lascano HR. 2009. Superoxide dismutase and glutathione reductase overexpression in wheat protoplast: photooxidative stress tolerance and changes in cellular redox state. Plant Growth Regulation **57**, 57–68.

Meskauskiene R, Nater M, Goslings D, Kessler F, Op den Camp R, Apel K. 2001. FLU: A negative regulator of chlorophyll biosynthesis in arabidopsis thaliana. Proceedings of the National Academy of Sciences of the United States of America **98**, 12826–12831.

Miller G, Schlauch K, Tam R, Cortes D, Torres MA, Shulaev V, Dangl JL, Mittler R. 2009. The plant NADPH oxidase RBOHD mediates rapid systemic signaling in response to diverse stimuli. Science Signaling **2**.

Munch D, Rodriguez E, Bressendorff S, Park OK, Hofius D, Petersen M. 2014. Autophagy deficiency leads to accumulation of ubiquitinated proteins, ER stress, and cell death in Arabidopsis. Autophagy **10**, 1579–1587.

Muñoz N, Robert G, Melchiorre M, Racca R, Lascano R. 2012. Saline and osmotic stress differentially affects apoplastic and intracellular reactive oxygen species production, curling and death of root hair during Glycine max L.–Bradyrhizobium japonicum interaction. Environmental and Experimental Botany **78**, 76–83.

Nakamura S, Hidema J, Sakamoto W, Ishida H, Izumi M. 2018. Selective Elimination of Membrane-Damaged Chloroplasts via microautophagy. Plant Physiology **177**, 1007–1026.

Nietzel T, Elsässer M, Ruberti C, *et al.* 2019. The fluorescent protein sensor roGFP2-Orp1 monitors in vivo H 2 O 2 and thiol redox integration and elucidates intracellular H 2 O 2 dynamics during elicitor-induced oxidative burst in Arabidopsis. New Phytologist **221**, 1649–1664.

Oikawa K, Goto-yamada S, Hayashi Y, *et al.* 2022. Pexophagy suppresses ROS-induced damage in leaf cells under high-intensity light.

Op Den Camp RGL, Przybyla D, Ochsenbein C, *et al.* 2003. Rapid Induction of Distinct Stress Responses after the Release of Singlet Oxygen in Arabidopsis. Plant Cell **15**, 2320–2332.

Pérez-Pérez ME, Couso I, Crespo JL. 2012*a*. Carotenoid deficiency triggers autophagy in the model green alga Chlamydomonas reinhardtii. Autophagy **8**, 376–388.

Pérez-Pérez ME, Lemaire SD, Crespo JL. 2012*b*. Reactive oxygen species and autophagy in plants and algae. Plant physiology **160**, 156–64.

Pérez-Pérez ME, Lemaire SD, Crespo JL. 2016. Control of Autophagy in *Chlamydomonas* Is Mediated through Redox-Dependent Inactivation of the ATG4 Protease. Plant Physiology **172**, 2219–2234.

Pérez-Pérez ME, Zaffagnini M, Marchand CH, Crespo JL, Lemaire SD. 2014. The yeast autophagy protease Atg4 is regulated by thioredoxin. Autophagy **10**, 1–12.

Qi H, Xia FN, Xiao S. 2021. Autophagy in plants: Physiological roles and post-translational regulation. Journal of Integrative Plant Biology **63**, 161–179.

Di Rienzo JA, Guzmán AW, Casanoves F. 2002. A multiple-comparisons method based on the distribution of the root node distance of a binary tree. Journal of Agricultural, Biological, and Environmental Statistics **7**, 129–142.

Robert G, Melchiorre M, Racca R, Trippi V, Lascano HR. 2009. Apoplastic superoxide level in wheat protoplast under photooxidative stress is regulated by chloroplast redox signals : Effects on the antioxidant system. Plant Science **177**, 168–174.

Robert G, Muñoz N, Alvarado-Affantranger X, Saavedra L, Davidenco V, Rodríguez-Kessler M, Estrada-Navarrete G, Sánchez F, Lascano R. 2018. Phosphatidylinositol 3-kinase function at very early symbiont perception: A local nodulation control under stress conditions? Journal of Experimental Botany **69**, 2037–2048.

Robert G, Yagyu M, Koizumi T, Naya L, Masclaux-Daubresse C, Yoshimoto K. 2021. Ammonium stress increases microautophagic activity while impairing macroautophagic flux in Arabidopsis roots. Plant Journal **105**, 1083–1097.

Rubin G, Tohge T, Matsuda F, Saito K, Scheible W-R. 2009. Members of the LBD Family of Transcription Factors Repress Anthocyanin Synthesis and Affect Additional Nitrogen Responses in Arabidopsis. The Plant Cell **21**, 3567–3584.

Scarpeci TE, Zanor MI, Carrillo N, Mueller-Roeber B, Valle EM. 2008. Generation of superoxide anion in chloroplasts of Arabidopsis thaliana during active photosynthesis : a focus on rapidly induced genes. Plant Mol Biol **66**, 361–378.

Scharfenberg M, Mittermayr L, Von Roepenack-Lahaye E, Schlicke H, Grimm B, Leister D, Kleine T. 2015. Functional characterization of the two ferrochelatases in Arabidopsis thaliana. Plant Cell and Environment **38**, 280–298.

Schwarzländer M, Dick TP, Meyer AJ, Morgan B. 2016. Dissecting redox biology using fluorescent protein sensors. Antioxidants and Redox Signaling **24**, 680–712.

Shibata M, Oikawa K, Yoshimoto K, Kondo M, Mano S, Yamada K, Hayashi M, Sakamoto W, Ohsumi Y, Nishimura M. 2013. Highly Oxidized Peroxisomes Are Selectively Degraded via Autophagy in Arabidopsis. The Plant cell **25**, 4967–83.

Signorelli S, Tarkowski ŁP, Van den Ende W, Bassham DC. 2019. Linking Autophagy to Abiotic and Biotic Stress Responses. Trends in Plant Science **24**, 413–430.

Su T, Li X, Yang M, Shao Q, Zhao Y, Ma C, Wang P. 2020. Autophagy: An Intracellular Degradation Pathway Regulating Plant Survival and Stress Response. Frontiers in Plant Science **11**, 1–16.

Trippi VS, Lascano HR, Melchiorre M. 2009. Plant senescence: A self-induced process. Current topics in plant biology **10**, 1–15.

Wang P, Wang T, Han J, Li M, Zhao Y, Su T, Ma C. 2021. Plant Autophagy : An Intricate Process Controlled by Various Signaling Pathways. Frontiers in Plant Science **12**, 754982.

Willems P, Mhamdi A, Stael S, Storme V, Kerchev P, Noctor G, Gevaert K, Van Breusegem F. 2016. The ROS wheel: Refining ROS transcriptional footprints. Plant Physiology **171**, 1720–1733.

Wintermans M. j. FG, De Mots A. 1965. SPECTROPHOTOMETRIC CHARACTERISTICS OF CHLOROPHYLLS a AND b AND THEIR PHEOPHYTINS IN ETHANOL. Biochimica et biophysica acta **109**, 448–453.

Woodson JD. 2019. Chloroplast stress signals: regulation of cellular degradation and chloroplast turnover. Current Opinion in Plant Biology **52**, 30–37.

Xiong Y, Contento AL, Bassham DC. 2007*a*. Disruption of Autophagy Results in Constitutive Oxidative Stress in Arabidopsis. Autophagy **3**, 257–258.

Xiong Y, Contento AL, Nguyen PQ, Bassham DC. 2007*b*. Degradation of oxidized proteins by autophagy during oxidative stress in Arabidopsis. Plant physiology **143**, 291–9.

Yang M, Bu F, Huang W, Chen L. 2019. Multiple regulatory levels shape autophagy activity in plants. Frontiers in Plant Science **10**, 1–7.

Yoshimoto K. 2012. Beginning to understand autophagy, an intracellular self-degradation system in plants. Plant & cell physiology **53**, 1355–65.

Yoshimoto K, Hanaoka H, Sato S, Kato T, Tabata S, Noda T. 2004. Processing of ATG8s , Ubiquitin-Like Proteins , and Their Deconjugation by ATG4s Are Essential for Plant Autophagy. The Plant Cell **16**, 2967–2983.

Yoshimoto K, Jikumaru Y, Kamiya Y, Kusano M, Consonni C, Panstruga R, Ohsumi Y, Shirasu K. 2009. Autophagy negatively regulates cell death by controlling NPR1-dependent salicylic acid signaling during senescence and the innate immune response in Arabidopsis. The Plant cell **21**, 2914–27.

Yoshimoto K, Ohsumi Y. 2018. Unveiling the molecular mechanisms of plant autophagy-from autophagosomes to vacuoles in plants. Plant and Cell Physiology **59**, 1337–1344.

Zheng X, Yang Z, Gu Q, Xia F, Fu Y, Liu P, Yin XM, Li M. 2020. The protease activity of human ATG4B is regulated by reversible oxidative modification. Autophagy **16**, 1838–1850.

Zhou J, Wang J, Cheng Y, Chi YJ, Fan B, Yu JQ, Chen Z. 2013. NBR1-Mediated Selective Autophagy Targets Insoluble Ubiquitinated Protein Aggregates in Plant Stress Responses. PLoS Genetics **9**.

Zhuang X, Cui Y, Gao C, Jiang L. 2015. Endocytic and autophagic pathways crosstalk in plants. Current Opinion in Plant Biology **28**, 39–47.

FIGURE LEGENDS

Figure 1: Autophagic flux and cytoplasmic redox state in *Arabidopsis thaliana* plants exposed to different abiotic stress conditions. (A-C) Seven-day old 35S:GFP-ATG8a transgenic plants and cytosol-targeted fluorescent redox sensors GFP2-Orp1 and GRX-roGFP2 expressing plants were exposed to different stress conditions in MS liquid medium. To induce autophagic bodies accumulation, MS liquid medium was supplemented with 1 µM Concanamycin A. (A) The stress treatments were performed for 16 h, followed by the evaluation of autophagic bodies accumulation (GFP-ATG8 columns) and the cytoplasmic redox state (GRX-roGFP and GFP2-Orp1 columns) by confocal microscopy. Arrowheads indicate autophagic bodies. GRX-roGFP and GFP2-Orp1 columns are ratiometric images. For pseudocolor display, the ratio was coded on a spectral color scale ranging from blue (fully reduced) to red (fully oxidized). Representative images are shown. The treatments included: MS with nitrogen (control), MS with nitrogen in darkness (-C), MS without nitrogen (-N), MS with nitrogen supplemented with 100 mM mannitol (Manitol), 50 mM NaCl (NaCl), 1 µM methyl viologen (MV) and 10 mM H2O2. (B) Average number of autophagic bodies accumulation per section. The average number of autophagic bodies was calculated from single-plane confocal images. Two sections from at least 7 plants were analyzed. (C) Average of cytoplasmic redox state expressed as the ratio of the fluorescence intensities measured at 488 nm and 405 nm (data expressed relative to the control condition). At least 6 plants were analyzed. Statistically significant differences are indicated by asterisks (**P* < 0.05; error bars: means ± SEM, DGC test).

Figure 2: Treatments with MV and H_2O_2 oxidized the cytoplasmic redox state and prevented autophagy induction in Arabidopsis. (A-C) Seven-day old 35S:GFP-ATG8a transgenic plants and cytosol-targeted fluorescent redox sensors GFP2-Orp1 and GRX-roGFP2 expressing plants were exposed to autophagy-inducing conditions and the effect of methyl viologen (MV) and H_2O_2 on autophagic flux and cytoplasmic redox state were analyzed. The stress treatments were performed for 16 h, followed by the evaluation of autophagic bodies accumulation (GFP-ATG8 columns) and the cytoplasmic redox state (GRX-roGFP and GFP2-Orp1 columns) by confocal microscopy. To induced autophagic bodies accumulation, MS liquid medium was supplemented with 1 µM Concanamycin A. Arrowheads indicate autophagic bodies. GRX-roGFP and GFP2-Orp1

columns are ratiometric images. For pseudocolor display, the ratio was coded on a spectral color scale ranging from blue (fully reduced) to red (fully oxidized). Representative images are shown. The treatments included: MS with nitrogen (control), MS with nitrogen in darkness (-C) supplemented with 10 mM H_2O_2 (-C + H_2O_2), MS without nitrogen (-N) supplemented with 1 µM methyl viologen (-N + MV) or 10 mM H_2O_2 (-N + H_2O_2). 10 mM Tiron and 10 mM Benzoic acid (BA) were used for ROS scavenging (-N + MV + Tiron and -N + MV + BA). (B) Average of autophagic bodies accumulation per section. The average of autophagic bodies number was calculated from single-plane confocal images. Two sections from at least 6 plants were analyzed. (C) Average of cytoplasmic redox state expressed as the ratio of the fluorescence intensities measured at 488 nm and 405 nm from single-plane confocal images (data expressed relative to control condition). At least 6 plants were analyzed. (D) Effects of oxidative treatments on the autophagic flux evaluated through the degradation of the GFP-ATG8a fusion protein by western blot. Seven-day old 35S:GFP-ATG8a transgenic Arabidopsis seedlings were exposed to the different treatments for 6 h. Total protein (40 µg) was subjected to immunoblot analysis with anti-GFP antibodies. The GFP-ATG8a fusion has a predicted molecular weight of approximately 40 kDa (closed arrowheads); free GFP has a predicted molecular weight of 27 kDa (open arrowheads). Representative images are shown. Ratio: the numbers in brackets denote the GFP/GFP-ATG8 ratio relativized to the condition without oxidative treatment. Three replicates were performed (more than fifty plants per replicate). HL: high light treatment (≈1000 µmoles m^{-2} s^{-1}). (E-G) Seven-day old Arabidopsis seedlings were exposed to 1 µM methyl viologen (MV), MV + 10 mM Tiron, MV + 10 mM BA, and control condition (without MV) for 8 h, and the different physiological parameters were analyzed. (E) Production of H_2O_2 and O_2^- revealed by *in situ* staining with 3′,3′-diaininobenzidine (DAB) and nitroblue tetrazolium (NBT), respectively; (F) quantum efficiency of PSII photochemistry (ΦPSII), and (G) Soluble sugar content. Asterisks indicate statistically significant differences (*$P < 0.05$; error bars: means ± SEM, DGC test)

Figure 3: Autophagy is induced after oxidative stress treatments in Arabidopsis. (A-D) Seven-day old transgenic plants expressing 35S:GFP-ATG8a and cytosol-targeted fluorescent redox sensors GFP2-Orp1 and GRX-roGFP2 were subjected to a brief exposure of oxidative stress, either 10 mM H_2O_2 or high light intensity (≈1000 µmoles m^{-2} s^{-1}), for 4 h. Subsequently they were transferred to MS liquid medium for a 20-hour recovery period under continuous light (120 µmoles m^{-2} s^{-1}) (recovery). Control plants were incubated under continuous light (120 µmoles m^{-2} s^{-1}) in H_2O_2-free MS liquid medium for 24 h. Stressed plants were incubated in MS supplemented with 10 mM H_2O_2 or high light intensity (≈1000 µmoles m^{-2} s^{-1}) for 24 h. (A) To induce accumulation of autophagic bodies, MS liquid medium was supplemented with 1 µM Concanamycin A. Arrowheads indicate autophagic bodies. GRX-roGFP and GFP2-Orp1 columns represent ratiometric images, with pseudocolor display indicating the ratio on a spectral color scale ranging from blue (fully reduced) to red (fully oxidized). Representative images are shown. (B) Average number of autophagic bodies accumulation per section. The average number of autophagic bodies was calculated from single-plane confocal images. Two sections from at least 6 plants were analyzed. (C) Average cytoplasmic redox state expressed as the ratio of the fluorescence intensities measured at 488 nm and 405 nm from single-plane confocal images (data are expressed relative to the control condition). At least 6 plants were analyzed. Asterisks indicate statistically significant differences (*$P < 0.05$; error bars: means ± SEM, DGC test). (D) Autophagic flux evaluated through the degradation of the GFP-ATG8a fusion protein by western blot. Total protein (40 µg) was subjected to immunoblot analysis with anti-GFP antibodies. The GFP-ATG8a fusion has a predicted molecular weight of approximately 40 kDa (closed arrowheads), while free GFP has a predicted molecular weight of 27 kDa (open arrowheads). Representative images are shown. The numbers in brackets denote the GFP/GFP-ATG8 ratio relativized to the control condition. Three replicates were performed (n > 50 plants per replicate). Asterisks indicate statistically significant differences (*$P < 0.05$; error bars: means ± SEM, DGC test).

Figure 4: DCMU and methylene blue treatments induced autophagic flux in Arabidopsis. (A-D) Seven-day old transgenic plants expressing 35S:GFP-ATG8a and cytosol-targeted fluorescent redox sensors GFP2-Orp1 and GRX-roGFP2 were incubated in MS medium supplemented with either 20 µM 3-(3,4-dichlorophenyl)-1,1-dimethylurea (DCMU) or 20 µM methylene blue (MB), and the autophagic flux and cytoplasmic redox state were evaluated. (A) Autophagic bodies accumulation and cytoplasmic redox state after 16 h of treatment. To induce autophagic bodies accumulation, MS liquid medium was supplemented with 1 µM Concanamycin A. Autophagic bodies are indicated by arrowheads. The GRX-roGFP and GFP2-Orp1 columns represent ratiometric images. For pseudo color display, the ratio was coded using a spectral color scale ranging from blue (fully reduced) to red (fully oxidized). Representative images are shown. (B) Average number of autophagic bodies per section. The average number of autophagic bodies was calculated from single-plane confocal images. Two sections from at least 5 plants were analyzed. (C) Average cytoplasmic redox state expressed as the ratio of the fluorescence intensities measured at 488 nm and 405 nm from single-plane confocal images (data expressed relative to control condition). Analysis was performed on at least 4 plants. Asterisks indicate statistically significant differences (*$P < 0.05$; error bars: means ± SEM, DGC test). (D) Evaluation of the effects of DCMU and MB on autophagic flux through degradation of the GFP-ATG8a fusion protein by western blot. Seven-day old transgenic Arabidopsis seedlings expressing 35S:GFP-ATG8a were exposed to the different treatments for 6 h. Total protein (40 µg) was subjected to immunoblot analysis with anti-GFP antibodies. The GFP-ATG8a fusion has a predicted molecular weight of approximately 40 kDa (closed arrowheads), while free GFP has a predicted molecular weight of 27 kDa (open arrowheads). Representative images are shown. The numbers in brackets denote the GFP/GFP-ATG8 ratio relative to the control condition. Four replicates were performed with more than fifty plants per replicate. (E) Seven-day old Arabidopsis seedlings were exposed to the different treatments for 6 h and soluble sugar content was analyzed. FW: fresh weight. Asterisks indicate statistically significant differences (*$P < 0.05$; error bars: means ± SEM, DGC test).

Figure 5: Autophagic flux is induced in conditionally chloroplast $^1O_2$-hyperproducing *flu* mutant Arabidopsis plants. (A-C) Seven-day old wildtype (Col-0) and *flu* mutant plants expressing 35S:GFP-ATG8a or GFP2-Orp1 were transferred to darkness for 8 h, followed by re-exposure to light. Control plants were maintained under continuous light conditions. After 8 h, the autophagic flux and cytoplasmic redox state were analyzed. (A) Autophagic bodies accumulation and cytoplasmic redox state. To induce autophagic bodies accumulation, the MS liquid medium was supplemented with 1 µM Concanamycin A. The GFP2-Orp1 columns represent ratiometric images. For pseudocolor display, the ratio was coded on a spectral color scale ranging from blue (fully reduced) to red (fully oxidized). Representative images are shown with arrowheads indicating autophagic bodies. (B) Average number of autophagic bodies accumulation per section. The average number of autophagic bodies was calculated from single-plane confocal images. Two different sections from at least 6 plants were analyzed. (C) Average cytoplasmic redox state expressed as the ratio of the fluorescence intensities measured at 488 nm and 405 nm from single-plane confocal images (data are expressed relative to Col-0 plants under control condition). At least 4 plants were analyzed. Asterisks indicate statistically significant differences (*$P < 0.05$; error bars: means ± SEM, DGC test). (D) Evaluation of autophagic flux through the degradation of the GFP-ATG8a fusion protein by western blot. Seven-day old wildtype (Col-0) and *flu* mutant plants expressing 35S:GFP-ATG8a were transferred to darkness for 8 h and then re-exposed to light for 6 h (after darkness). Continuous light was used as a control (light). Total protein (40 µg) was subjected to immunoblot analysis with anti-GFP antibodies. The GFP-ATG8a

fusion has a predicted molecular weight of approximately 40 kDa (closed arrowheads); while free GFP has a predicted molecular weight of 27 kDa (open arrowheads). Representative images are shown. The numbers in brackets denote the GFP/GFP-ATG8 ratio relative to *flu* mutans under control condition. Three replicates were performed (more than fifty plants per replicate). Asterisks indicate statistically significant differences.

Supplementary Figure 1: (A) Effects of 10 µM MV on ROS generation. After 2 h, MV-treated plants exhibit a significant accumulation of ROS. The co-administration of tiron led to a reduction in ROS generation. After 4 h, plants treated with MV did not show ROS production, indicating cell death. However, co-administration of tiron conferred resistance to the oxidative treatment, as evidenced by the observed ROS production. (B-D) Autophagic flux and cytoplasmic redox state in Arabidopsis plants exposed to different MV concentrations. Seven-day old 35S:GFP-ATG8a transgenic plants and cytosol-targeted fluorescent redox sensors GFP2-Orp1 and GRX-roGFP2 expressing plants were exposed to different MV concentrations. To induce autophagic bodies accumulation, MS liquid medium was supplemented with 1 µM Concanamycin A. The stress treatments were performed for 16 h, followed by the evaluation of autophagic bodies accumulation (GFP-ATG8 columns) and the cytoplasmic redox state (GRX-roGFP and GFP2-Orp1 columns) by confocal microscopy. GRX-roGFP and GFP2-Orp1 columns are ratiometric images. For pseudocolor display, the ratio was coded on a spectral color scale ranging from blue (fully reduced) to red (fully oxidized). Representative images are shown. (C) Average of autophagic bodies accumulation per section. The average of autophagic bodies number was calculated from single-plane confocal images. Two sections from at least 3 plants were analyzed. (D) Average of cytoplasmic redox state expressed as the ratio of the fluorescence intensities measured at 488 and 405 (data expressed relative to 0 µM MV). At least 3 plants were analyzed.

Supplementary Figure 2: (A-B) Cytoplasmic oxidation of the GSH:GSSG sensor probe (GRX-roGFP2) in Arabidopsis plants exposed to different H_2O_2 concentrations. Seven-day old GRX-roGFP2 expressing plants were exposed to different H_2O_2 concentrations. The stress treatments were performed for 6 h, followed by the evaluation of the cytoplasmic redox state (GRX-roGFP) by confocal microscopy. For pseudocolor display, the ratio was coded on a spectral color scale ranging from blue (fully reduced) to red (fully oxidized). Representative images are shown. (B) Average of cytoplasmic redox state expressed as the ratio of the fluorescence intensities measured at 488 and 405 (data expressed relative to 0 µM H_2O_2). At least 3 plants were analyzed. (C) Autophagic flux evaluated through the degradation of the GFP-ATG8a fusion protein by western blot. Seven-day old 35S:GFP-ATG8a expressing plants were exposed to different H_2O_2 concentrations. Total protein (40 µg) was subjected to immunoblot analysis with anti-GFP antibodies. The GFP-ATG8a fusion has a predicted molecular weight of approximately 40 kDa (closed arrowheads); free GFP has a predicted molecular weight of 27 kDa (open arrowheads). Representative images are shown. Ratio: the numbers in brackets denote the GFP/GFP-ATG8 ratio relativized to the condition without oxidative treatment (to 0 µM H_2O_2).

Supplementary Figure 3: Effects of DTT and tiron on ROS production, cytoplasmic oxidation of the GSH:GSSG sensor probe (GRX-roGFP2), and autophagic flux in Arabidopsis plants exposed to 1 µM MV. (A) Production of H_2O_2 revealed by *in situ* staining with 3′,3′-diaininobenzidine (DAB staining) and cytoplasmic redox state (GRX-roGFP2). GRX-roGFP column is a ratiometric image.

For pseudocolor display, the ratio was coded on a spectral color scale ranging from blue (fully reduced) to red (fully oxidized). Representative images are shown. At least 3 plants were analyzed. (B) Autophagic flux evaluated through the degradation of the GFP-ATG8a fusion protein by western blot. Seven-day old 35S:GFP-ATG8a expressing plants were exposed to the different treatments. Total protein (40 µg) was subjected to immunoblot analysis with anti-GFP antibodies. The GFP-ATG8a fusion has a predicted molecular weight of approximately 40 kDa (closed arrowheads); free GFP has a predicted molecular weight of 27 kDa (open arrowheads). Representative images are shown. Ratio: the numbers in brackets denote the GFP/GFP-ATG8 ratio relativized to the control condition. N: nitrogen; MV: methyl viologen; DTT: dithiothreitol.

Supplementary Figure 4: Sequence alignment of ATG4 proteases from different organisms including *Saccharomyces cereviseae* (QHB11163.1), *Homo sapiens* (ATG4A- NP_001308219.1, ATG4B, NP_847896.1) *Chlamydomonas reinhardtii* (Cre12.g510100.t1.1), *Arabidopsis thaliana* (ATG4A- AT2G44140.1, ATG4B- AT3G59950.1), *Marchantia polymorpha* (Mapoly0153s0038.1.p) and *Physcomitrium patens* (ATG4A- Pp3c11_22820V3.1.p, ATG4B, Pp3c7_280V3.1.p). In orange is labeled the conserved active site (WGCT/ML/IR) of these proteases including the catalytic Cys77 (number according to HsATG4A) that is essential for ATG4 activity (Tanida et al., 2004). Note that HsATG4A and HsATG4B contain two conserved cysteine residues Cys81 and Cys92, or Cys78 and Cys89 (numbers according to HsATG4A or HsATG4B, respectively, black arrows), but these cysteine residues are not conserved in yeasts or other eukaryotes as algae or plant ATG4s. H_2O_2, at the site of Cys81/Cys78, is an oxidative signal that inactivates the delipidation activity of ATG4 at the site of autophagosome formation promoting lipidation of ATG8. In the case of HsATG4B, Cys292 and Cys361 (Cys labeled in red) which are not conserved in other species, are regulated by redox signals to influence ATG4B activity and autophagy. In yeast ATG4, its activity is redox regulated by oxidoreduction of a single disulfide bond between Cys-338 and Cys-394 (Cys labeled in blue). In Chlamydomonas, Cys400 is identified as the key site participating in Atg4 redox regulation (Cys labeled in green).

Supplementary Figure 5: (A) Sequence alignment of ATG3 proteins from different organisms including *Saccharomyces cerevisiae* (QHB11385.1), *Homo sapiens* (NP_001265641.1), *Chlamydomonas reinhardtii* (Cre02.g102350_4532.1), *Arabidopsis thaliana* (AT5G61500.1), *Marchantia polymorpha* (Mapoly0003s0208.1.p) and *Physcomitrium patens* (Pp3c8_11900V3.1.p). The catalytic Cys264 (number according to HsATG3) is conserved in all proteins studied (black box with a black arrow). (B) Sequence alignment of ATG7 proteins from different organisms including *Saccharomyces cerevisiae* (QHB09162.1), *Homo sapiens* (NP_001336161.1), *Chlamydomonas reinhardtii* (Cre03.g165215.t1.1), *Arabidopsis thaliana* (AT5G45900.1), *Marchantia polymorpha* (Mapoly0015s0071.1.p) and *Physcomitrium patens* (Pp3c24_8100V3.1.p). The catalytic Cys572 (number according to HsATG7) is conserved in all proteins studied (black box with a black arrow). Other potential cysteine residues which are conserved may serve as potential candidates for further investigation. Under nonreducing conditions, when ATG3 and ATG7 enzymes are inactive, form stable thioester complexes with LC3 (ATG8). Under pro-oxidizing conditions, loss in this stable interaction with LC3 during active autophagy sensitizes ATG3 and ATG7 to thiol oxidation and leads to the formation of an intermolecular disulfide-bound complex between the Cys264 from ATG3 and the Cys572 from

ATG7, which inhibit ATG8 lipidation (Frudd et al., 2018). Other cysteine residues which are conserved (black boxes) are potential candidates for further studies.

Supplementary Figure 6: Characterization of *fc2* and *flu* mutant plants under continuous light conditions (control conditions). Wild type (Col-0), *fc2* and *flu* mutant plants were grown 7 days under continuous light conditions and different growth and physiological parameters were evaluated. (A) Production of H_2O_2 was revealed by *in situ* staining with 3′,3′-diaininobenzidine (DAB); autophagic bodies accumulation (GFP-ATG8 columns) and the cytoplasmic redox state (GFP2-Orp1 column) analyzed by confocal microscopy. To induced autophagic bodies accumulation (GFP-ATG8 column), MS liquid medium was supplemented with 1 µM Concanamycin A. GFP2-Orp1 column is a ratiometric image. For pseudocolor display, the ratio was coded on a spectral color scale ranging from blue (fully reduced) to red (fully oxidized). Representative images are shown. At least 4 plants were analyzed. Bar plots show the average number of autophagic bodies and the average of cytoplasmic redox state. The average of autophagic bodies number was calculated from single-plane confocal images. Two sections from at least 4 plants were analyzed. The average of cytoplasmic redox state is expressed as the ratio of the fluorescence intensities measured at 488 and 405 (data expressed relative to Col-0). At least 4 plants were analyzed. (B) Average root length, soluble sugar, chlorophyll and MDA content in the different genotypes after growing seven days under continuous light conditions (*$P < 0.05$; error bars: means ± SEM, DGC test).

Supplementary Figure 7: Transcript level of *Atg* genes in Arabidopsis plants subjected to different oxidative treatments. (A) Seven-day old wild type Arabidopsis plants (Col-0) were exposed to oxidative stress conditions for 4 h (10 mM H_2O_2, 1 µM methyl viologen (MV), 1 µM methyl viologen + 10 mM tiron (MV + Tiron)), followed by the analysis of the transcript levels of *Atg* genes through RT-qPCR. Data are relative to control condition (assigned a value of 1). (B) Seven-day old *flu* mutant plants grown under continuous light conditions were exposed to darkness for 8 h and re-exposed to light for 8 h or kept in continuous light (control), and the expression of *Atg* genes were analyzed by RT-qPCR. Data are relative to Col-0 genotype (assigned a value of 1). (C) Publicly available microarray data were utilized to compare the expression of *Atg* genes under various conditions, including nitrogen deficiency (Rubin *et al.*, 2009), treatment with 10 mM H_2O_2 for 24 h (Willems *et al.*, 2016), treatment with 10 µM MV for 2 h (Scarpeci *et al.*, 2008), and the examination of *flu* mutant plants subjected to an 8-hour cycle of darkness followed by 2 h of light (Op Den Camp *et al.*, 2003). Expression values were normalized to the corresponding control conditions employed in each study and were expressed as $\log_2$ values.

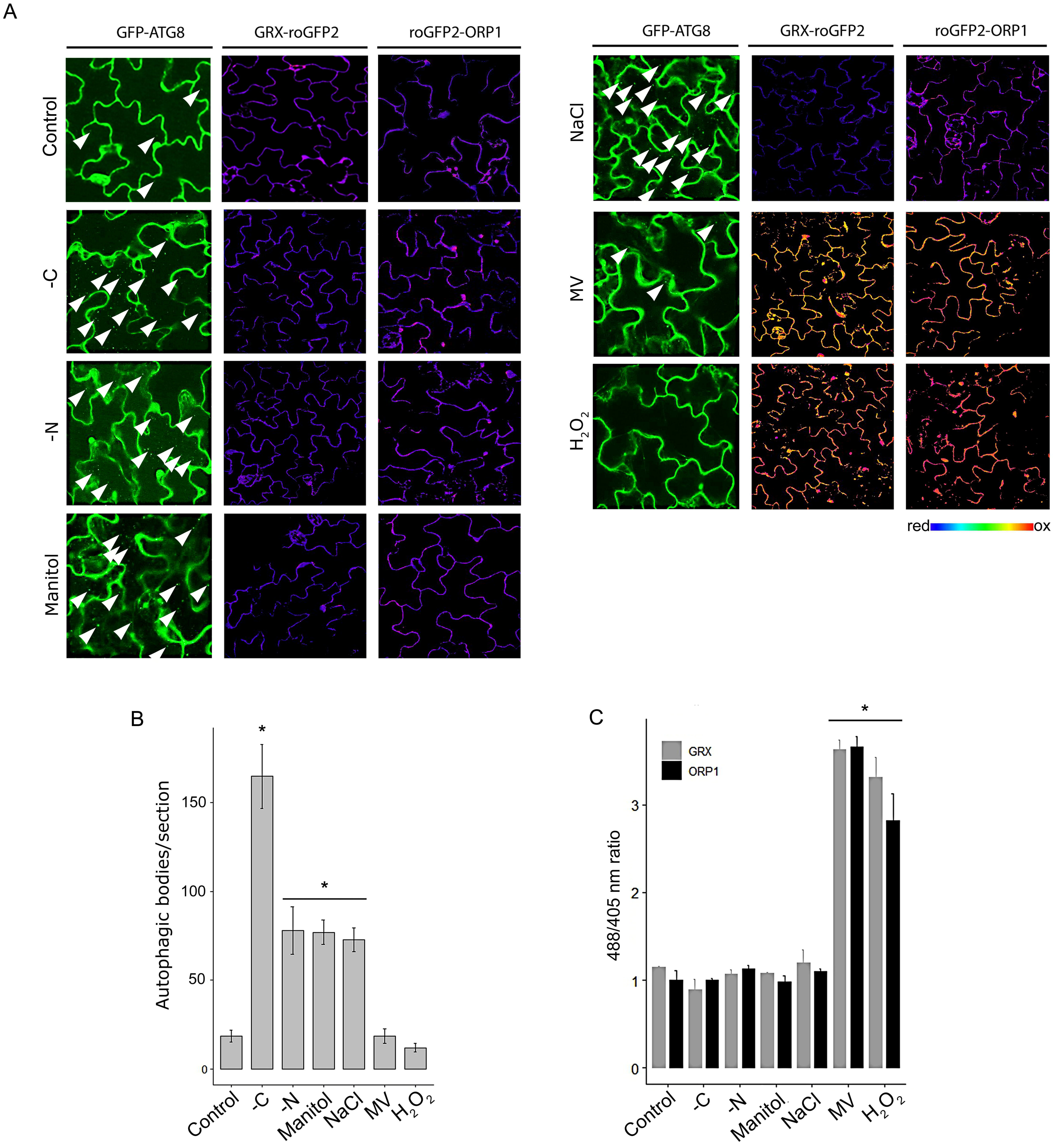
A
GFP-ATG8
GRX-roGFP2
roGFP2-ORP1
Control
-C
-N
Manitol
GFP-ATG8
GRX-roGFP2
roGFP2-ORP1
NaCl
MV
H2O2
red
ox
B
Autophagic bodies/section
150
100
50
0
*
*
Control
-C
-N
Manitol
NaCl
MV
H2O2
C
*
GRX
ORP1
488/405 nm ratio
3
2
1
0
Control
-C
-N
Manitol
NaCl
MV
H2O2

A
GFP-ATG8
GRX-roGFP2
roGFP2-ORP1
Control
-N
-C
-C + H_2O_2
-N + H_2O_2
-N + MV
-N + MV + Tiron
-N + MV + BA
red
ox
B
Autophagic bodies/section
400
300
200
100
0
*
Control
-N
-N + H_2O_2
-N + MV
-N + MV + Tiron
-N + MV + BA
-C
-C + H_2O_2
C
Sensor
GRX
ORP1
405/488 nm ratio
4
3
2
1
0
D
Control
-N
-C
MV
H_2O_2
Tiron
BA
HL
GFP-ATG8
GFP
ratio
(1)
(1,1)
(0,28)*
(0,2)*
(0,4)*
(3,78)*
(3,06)*
(1,15)
(0,94)
E
MV
MV+Tiron
MV+BA
NBT staining
DAB staining
F
ΦPSII
0.8
0.6
0.4
0.2
Time after treatment (h)
0
2
4
6
8
Control
MV
MV+Tiron
MV+BA
G
Soluble sugars (µg/mg FW)
2,0
1,6
1,2
0,8
0,4
0,0
Control
Dark
MV
MV+Tiron

A
GFP-ATG8
GRX-roGFP2
roGFP2-ORP1
Control
H2O2 (24h)
Recovery
red
ox
B
Autophagic bodies/section
0
20
40
60
80
*
*
Control
H2O2 (24 h)
Recovery
C
405/488 ratio
0
1
2
3
*
GRX
ORP1
Control
H2O2 (24 h)
Recovery
D
Control
H2O2 (24 h)
Recovery
Control
HL
Recovery
GFP-ATG8 ▶
GFP ▷
ratio
(0,92)
(0,32)*
(1,97)*
(0,94)
(0,56)*
(4,63)*

A
GFP-ATG8
GRX-roGFP2
roGFP2-ORP1
Control
DCMU
MB
red
ox
B
Autophagic bodies/section
0
25
50
75
*
*
Control
DCMU
MB
C
GRX
ORP1
405/488 ratio
0
1
2
3
Control
DCMU
MB
D
DCMU - - + +
MB - - - -
- - - -
- - + +
GFP-ATG8
GFP
ratio
(0,91)
(2,78)*
(0,99)
(2,36)*
E
Soluble sugars (μg/mg FW)
0,0
0,4
0,8
1,2
1,6
2,0
*
*
Control
Dark
DCMU
MB

A
Col-0 background
flu background
GFP-ATG8
roGFP2-ORP1
GFP-ATG8
roGFP2-ORP1
Continuous light
After darkness
red
ox
B
Continuous light
After darkness
Autophagic bodies/section
140
120
100
80
60
40
20
0
*
flu
Col-0
flu
C
Continuous light
After darkness
405/488 ratio
3
2
1
0
flu
Col-0
flu
D
Light
After darkness
flu
Col-0
flu
GFP-ATG8
GFP
ratio
(0,91)
(0,89)
(2,27)*